Processing and Application of Ceramics 14 [2] (2020) 113–118
https://doi.org/10.2298/PAC2002113U

Low-temperature hydrothermal synthesis of hierarchical flower-like CuB_2O_4 superstructures

Daniel Ursu[1], Anamaria Dabici[1], Marinela Miclau[1], Nicolae Miclau[2,*]

[1]*National Institute for Research and Development in Electrochemistry and Condensed Matter, Timisoara, Dr. A. Păunescu-Podeanu no. 144, 300569, Timisoara, Romania*
[2]*Politehnica University Timisoara, Str. Piata Victoriei, no. 2, 300006, Timisoara, Romania*

Received 21 November 2019; Received in revised form 30 January 2020; Accepted 22 March 2020

Abstract

We report for the first time the fabrication of hierarchical ordered superstructure CuB_2O_4 with flower-like morphology via a one-step, low temperature hydrothermal method. The tetragonal structure of CuB_2O_4 was determined by X-ray diffraction and high-resolution transmission electron microscopy. Optical measurements attested of the quality of the fabricated CuB_2O_4 and high temperature X-ray diffraction confirmed its thermal stability up to 600 °C. The oriented attachment growth and the hierarchical self-assembly of micrometer-sized platelets producing hierarchical superstructures with flower-like morphology are designed by pH of the hydrothermal solution. The excellent band gap, high thermal stability and hierarchical structure of the CuB_2O_4 are promising for the photovoltaic and photocatalytic applications.

Keywords: *copper metaborate, hierarchical structure, flower-like morphology, hydrothermal method*

I. Introduction

The ability to control and manipulate the geometrical parameters of materials (size and shape) is one of the challenging issues in materials science. The development of efficient synthetic routes to obtain well-defined morphologies is important task [1–4], as hierarchical superstructures could be a way to design the physical and chemical properties of a material.

Copper borate has been extensively studied for their magnetic properties [5,6] and especially for the applications in photocatalytic water splitting [7]. Recently, the gigantic direction dependent luminescence and the possibility of introducing crystal chirality by a weak magnetic field and the magnetic field found in the copper borate showed that this material is still actual for the development of the new applications [8,9].

To the best of our knowledge, the synthesis methods reported for CuB_2O_4 require high pressures and temperatures under thermal conditions [10–12], precipitation reaction in aqueous solution with modifying agent [13] or hydrothermal synthesis in alkaline solution [14]. So far, the morphologies of the copper borates obtained by different methods were ellipsoidal [13], round and rod-like in shape [14].

In this context, we revisited the CuB_2O_4 system using hydrothermal synthesis in acidic medium and thus the fabrication of the hierarchically ordered superstructure CuB_2O_4 with flower-like morphology is reported for the first time.

II. Experimental procedure

Copper precursor (Cu) and boron precursor (B_2O_3) were purchased from Sigma-Aldrich and used without any prior purification. In a typical synthesis process, the desired copper and boron precursors quantities were mixed in water and pH = 4 has been established using acetic acid. The molar ratio of metals Cu:B varied from 1:2 to 1:10. The obtained suspension was transferred into Teflon-line autoclave with a volume of 60 ml. The fill factors of the autoclave were in the range of 10 to 30%. Samples were prepared in the temperature range from 150 to 250 °C during the reaction time between 12 and 60 h. The autoclave was cooled down to room temperature naturally. The precipitates were separated by the filtration using MN 640 de ⌀125 mm filter paper, then washed with deionized water and dried at 80 °C for 1 h.

*Corresponding author: tel: +40 726182521,
e-mail: *nicolae.miclau@upt.ro*

The structure of the products was determined by powder X-ray diffraction (XRD) PW 3040/60 X'Pert PRO using Cu-Kα radiation with λ = 1.5418 Å, in the range 2θ = 10–80°. The morphology of the CuB_2O_4 powder was observed using scanning electron microscope (Inspect S, SEM/EDX) and transmission electron microscope (TEM, Titan G2 80-200). The TEM specimens were prepared by crushing powder samples under ethanol in an agate mortar and depositing the drops onto a holey carbon membrane supported by a copper grid. The *d*-spacing of the lattice was calculated using fast Fourier transform (FFT) image obtained by NIH's ImageJ software. The topography and particle size of the samples were investigated by AFM (Model Nanosurf® EasyScan 2 Advanced Research). UV-visible diffuse reflectance spectra of the powdered samples were analysed by using a spectrophotometer (LAMBDA 950 UV/Vis/NIR Spectrophotometer, PerkinElmer, wavelength range up to 3300 nm). Micro Raman measurements were performed on Nanonics Raman module mounted on optical microscope (Olympus) using Raman excitation given by argon laser Stellar Pro Modulaser with selected wavelength of 514 nm. Raman signal was detected using ANDOR SR 500i-A-R spectrometer equipped with CCD.

The electrochemical investigations were performed using a Voltalab potentiostat model PGZ 402, with VoltaMaster 4 (version 7.09) software. A single compartment three-electrode cell based on a platinum wire as counter electrode, Ag/AgCl/KCl sat. electrode coupled to a Luggin capillary as reference electrode and CuB_2O_4 thin film as working electrode (area 0.28 cm^2) were used. The synthesized CuB_2O_4 powder was mixed with 5 wt.% polyvinylidene fluoride (PVDF) in N-methyl-2-pyrrolidone (NMP) solution and the obtained paste was coated on the FTO substrate using doctor-blade technique. All potentials were referenced to the standard hydrogen electrode (SHE). The capacitance of the interface was measured using 0.1 mol/l Na_2SO_4 aqueous solutions with pH = 7, in the potential range from −0.6 to −0.1 V with a 25 mV potential step at 1 kHz and AC potential amplitude of 20 mV. The thermal stability of the obtained CuB_2O_4 structures was studied by in situ XRD using a variable temperature chamber (Anton Paar HTK 2000 high temperature chamber). The diffraction patterns were recorded in 2θ angular range 10–80° using a heating rate of 10 °C/min.

III. Results and discussion

The following specific conditions: 1:2 molar ratio of $Cu:B_2O_3$, pH = 4, 250 °C and 48 h were used to obtain pure copper metaborate CuB_2O_4. In accordance with the Eh-pH diagram and pC-pH diagram for the system B−O−H and Cu−O−H, under acidic pH, hydroxo Cu(II) complexes and H_3BO_3(aq) are thermodynamically favourable [15,16]. Thus, for certain temperature, pH, reaction time and molar ratio of Cu:B, the stability of $Cu(OH)_3^-$ and $B(OH)_3$(aq) species is realized, the supersaturation is reached and CuB_2O_4 is obtained.

Figure 1 shows X-ray diffraction pattern of the CuB_2O_4 compound prepared by the hydrothermal method. All the diffraction peaks could be indexed as CuB_2O_4 with tetragonal structure (space group: $I\bar{4}2d$, JCPDS Nr. 01-070-2446).

The SEM image (Fig. 2a) of the CuB_2O_4 sample shows an unexpected morphology, namely flower-like

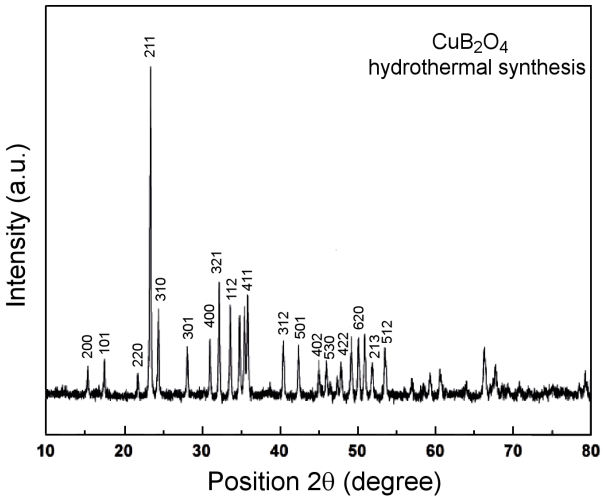

Figure 1. XRD pattern of CuB_2O_4 powder obtained by hydrothermal method

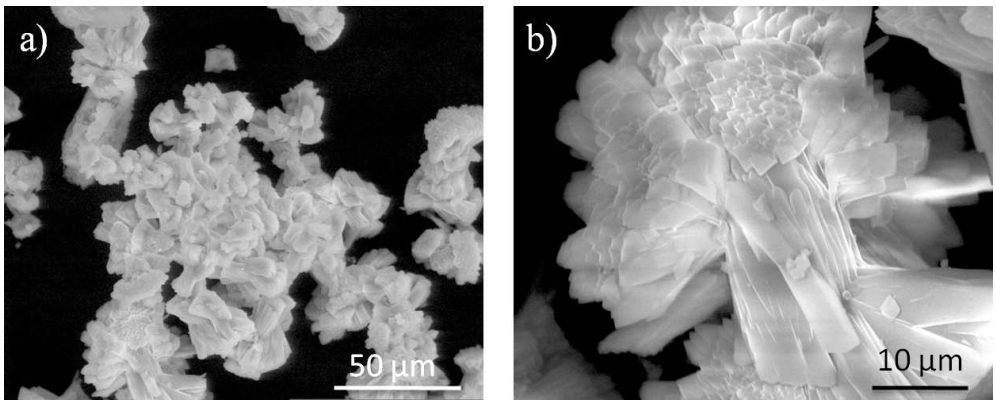

Figure 2. SEM image of the CuB_2O_4 product (a) and a hierarchically ordered CuB_2O_4 superstructure with flower-like morphology (b)

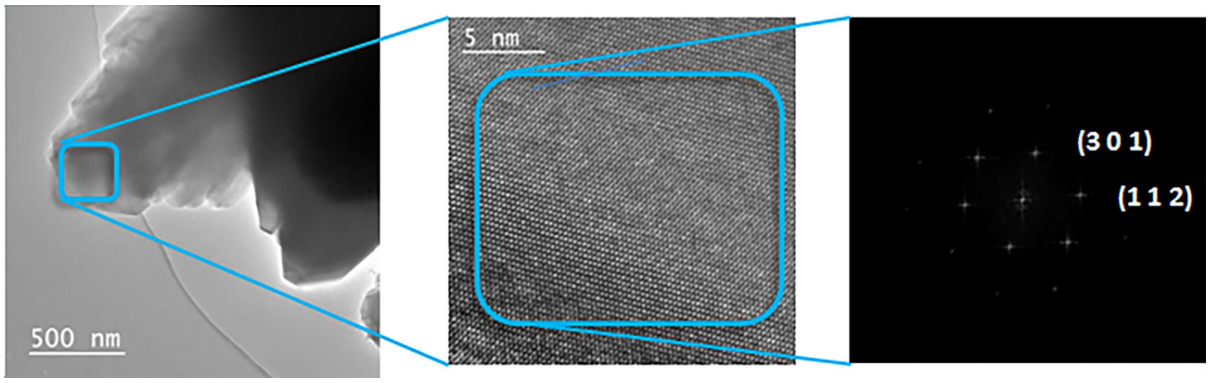

Figure 3. TEM (a) and HR-TEM (b) images of CuB_2O_4 thin platelets and *d*-spacing calculated using FFT obtained by NIH's ImageJ software (c)

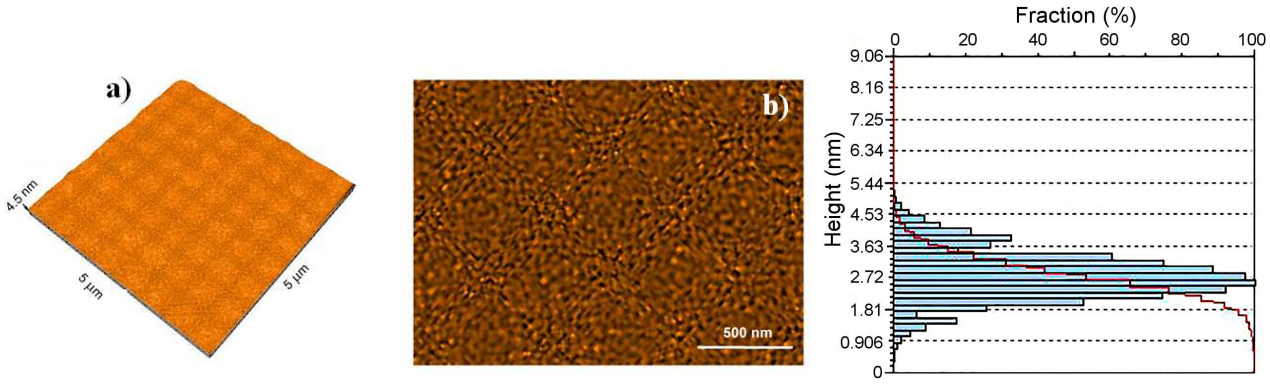

Figure 4. AFM images of CuB_2O_4 thin platelets (a), enlarged AFM image of 2D micrometric square structures (b) and height distribution for 2D micrometric square structures extracted from the AFM image (c)

hierarchical structures, which are built by self-assembly of the thin platelets (Fig. 2b).

In addition, HR-TEM analysis of the thin platelets was used to determine the crystal lattice and to confirm CuB_2O_4 single phase identified by the XRD study. At first, the *d*-spacing of the CuB_2O_4 lattice was calculated using Fast Fourier transform (FFT) image obtained by NIH's ImageJ software. In Fig. 3, the d-spacing of the lattice fringes calculated from FFT image (inset) was found to be 3.2 Å and 2.6 Å. These values are consistent with the standard PDF 01-070-2446 values of (301) crystal plane (i.e. 3.16 Å) and (112) crystal plane (i.e. 2.65 Å) of tetragonal CuB_2O_4 revealing to be perfectly single crystalline.

In order to study in-depth the growth of the copper borates in platelet-like morphology, AFM analysis was performed. AFM image (Fig. 4a) revealed that these thin platelets are built by self-assembly of 2D square structures with 1 µm side. Furthermore, the enlarged AFM image (Fig. 4b) highlights that 2D micrometric square structures are themselves built from the nanoparticles with the height distribution presented in Fig. 4c.

In order to further investigate the optical properties of the 3D flower-like CuB_2O_4 hierarchical structures, UV-visible characterizations were performed. UV-visible absorption spectrum is shown in Fig. 5a. The CuB_2O_4 exhibits a band absorption edge at 315 nm and an intense absorption peak near 635 nm. The latter peak is associated with the *d–d* transition absorptions of Cu^{2+} [17].

The optical direct band gap of the CuB_2O_4 was estimated from the equation $(\alpha h\nu)^2 = A(h\nu - E_g)$ where α, ν, A and E_g are the absorption coefficient, the frequency of light, a constant and the band gap, respectively [18,19]. The optical band gap of the prepared CuB_2O_4 was estimated from the $(\alpha h\nu)^2$ *vs.* $h\nu$ plot to be 3.61 eV (Fig. 5b), which is higher than 3.29 eV reported in earlier studies [6]. The increase in the band gap energy could be explained by the reduction of the crystal-size, also highlighted by AFM analysis.

The Raman spectrum of the prepared CuB_2O_4 (Fig. 6) shows three bands at 298, 344 and 630 cm^{-1}. In accordance with earlier studies, the bands below 800 cm^{-1} in copper borates are assigned to the bending vibrations of tetrahedral BO_4 groups and vibrations related to Cu–O bond [20].

The Mott-Schottky analysis of the CuB_2O_4 sample is presented in Fig. 7, where the linear part of the curve is extrapolated to $1/C^2 = 0$ and the values of V_{fb} are estimated to be 0.505 V *vs. SHE*. The donor concentration (N_D) was obtained by the Mott-Schottky equation [21]:

$$\frac{1}{C^2} = \frac{2}{e \cdot \varepsilon \cdot \varepsilon_0 \cdot N_D \cdot A^2}\left(V - V_{fb} - \frac{k \cdot T}{e}\right) \quad (1)$$

where C represents the capacitance of the space charge

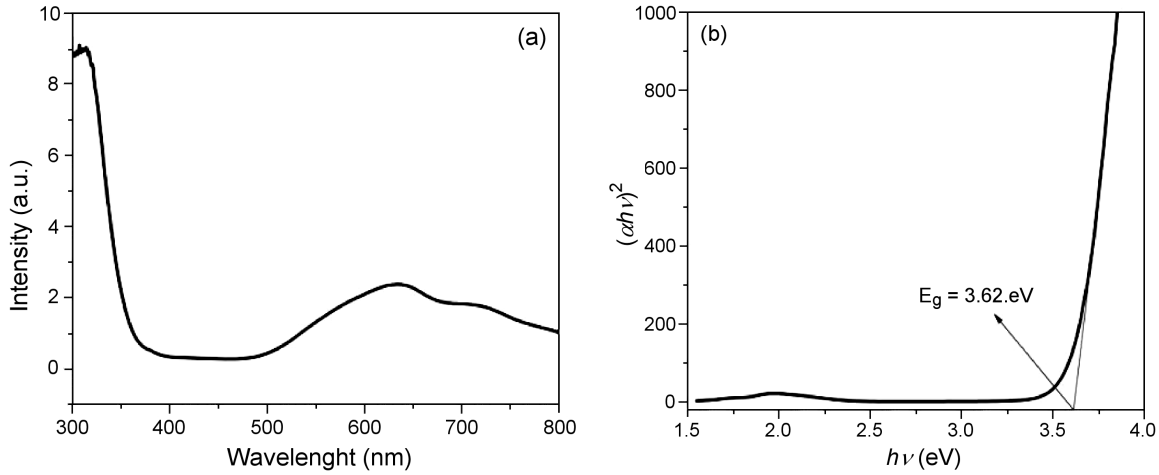

Figure 5. UV-visible absorbance spectrum of the hierarchically ordered superstructure CuB_2O_4 (a) and band gap of CuB_2O_4 calculated from the diffuse reflectance spectrum (b)

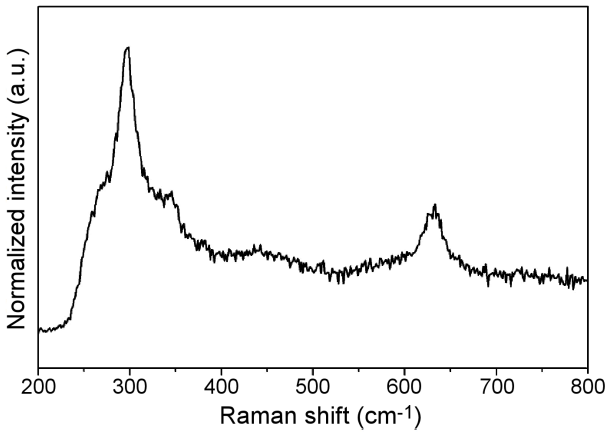

Figure 6. Raman spectra of CuB_2O_4 sample

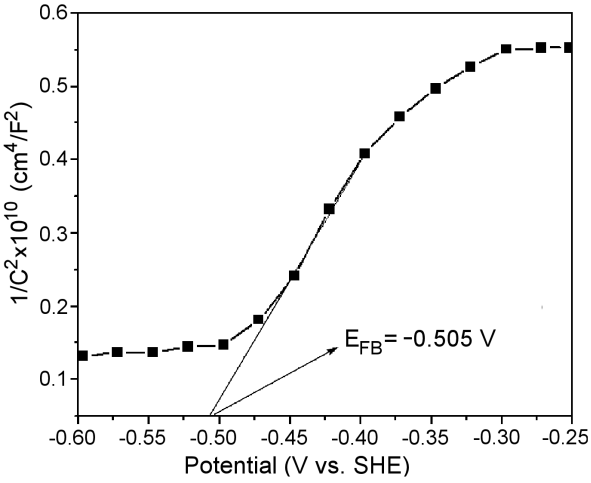

Figure 7. M-S plots of the hierarchical ordered superstructure CuB_2O_4

region, ε_0 is the vacuum permittivity, ε is the dielectric constant of the CuB_2O_4, e is the electron charge, A is the surface area of the semiconductor/electrolyte interface, V is the electrode applied potential, k is the Boltzmann constant, T is the absolute temperature, N_D is the donor concentration and V_{fb} is the flat-band potential of the semiconductor. The positive slope of the Mott-Schottky plot confirmed n-type conductivity of the CuB_2O_4.

According to the M-S relationship, the donor density value (N_D) of 9.68×10^{18} cm^{-3} was calculated from the slope of the linear region (Fig. 7), assuming that dielectric constant of the CuB_2O_4 is 6 in the following equation [21]:

$$N_D = \frac{2}{e \cdot \varepsilon \cdot \varepsilon_0} \left[\frac{\mathrm{d}\left(C^{-2}\right)}{\mathrm{d}V} \right]^{-1} \qquad (2)$$

In situ XRD patterns, presented in Fig. 8, show the phase evolution of the prepared CuB_2O_4 in the temperature range from 25 to 600 °C in air. The thermal stability of the CuB_2O_4 compound in air was confirmed in the whole temperature range up to 600 °C. In addition, no effect of temperature on the morphology was observed, i.e. the flower-like hierarchical superstructures show high stability even at 600 °C (Fig. 9).

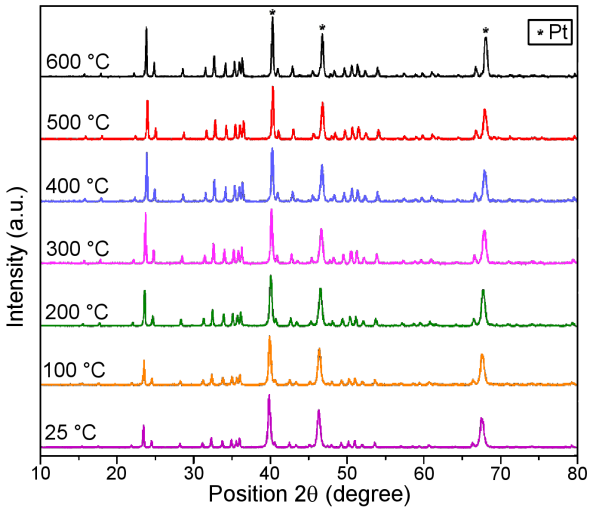

Figure 8. High temperature X-ray diffraction patterns showing phase evolution CuB_2O_4 compound in air

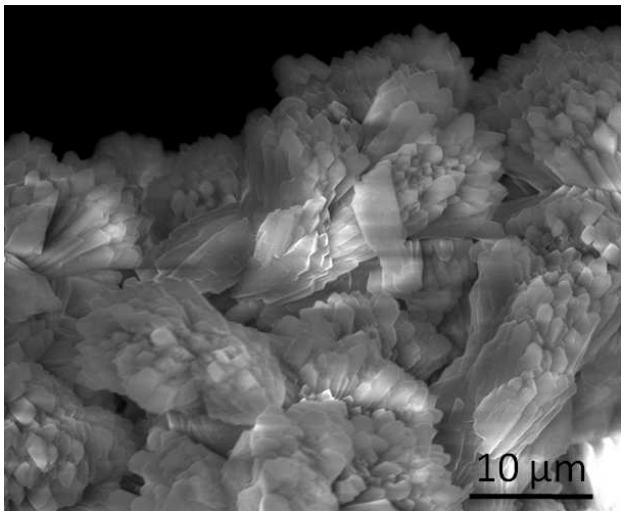

Figure 9. SEM image of CuB_2O_4 compound obtained after thermal treatment in XRD high temperature chamber

The good agreement between SEM and AFM observations of the copper borate prepared in acid medium suggests the occurrence of oriented attachment (OA) mechanism to explain the formation of micrometer-size square structures based on the coalescence of nanoparticles as building blocks. In accordance with the model proposed by Ribeiro *et al.* [22], oriented attachment growth occurs by effective collisions between particles with the same orientation in order to minimize the surface energies. Hydrothermal medium provides a very high degree of freedom for rotation and translation motions of dispersed particles and the frequency of the oriented collisions is high.

The formation of the thin platelets by the self-assembly of micrometer-size square structures followed by their self-assembly in the hierarchical superstructures with the flower-like morphology is proposed as the formation mechanism of these copper borates. Owing to the acid hydrothermal solution, the difference of the surface energy between crystal planes leads to the preferential growth. But without a theoretical modelling of the surface energy corresponding to each crystal plane, an in-depth study of the formation mechanism is difficult.

IV. Conclusions

We report for the first time the fabrication of hierarchically ordered superstructure CuB_2O_4 with flower-like morphology via a one-step low temperature hydrothermal method. The results revealed that the hierarchical self-assembly of micrometer-sized platelets producing hierarchical superstructures with the flower-like morphology are designed by pH of the hydrothermal solution, as a way to minimize energy in the specific crystallographic planes. High temperature X-ray diffraction analysis has revealed a high thermal stability of CuB_2O_4 up to 600 °C. The excellent band gap, high thermal stability and hierarchical structure of the CuB_2O_4 are promising for the photovoltaic and photocatalytic applications.

Acknowledgement: This work was supported by the Romanian National Authority for Scientific Research and Innovation, CNCS – UEFISCDI under Grant project number PN-III-P2-2.1-PED-2016-0526, within PNCDI III.

References

1. R.S. Liu, *Controlled Nanofabrications: Advances and Applications*, Jenny Stanford Publishing, Singapore, 2012.
2. S. Kumar, K. Singh, M. Miclau, Ch. Simon, C. Martin, A. Maignan, "From spin induced ferroelectricity to spin and dipolar glass in a triangular lattice: The $CuCr_{1-x}V_xO_2$ ($0 \leq x \leq 0.5$) delafossite", *J. Solid State Chem.*, **203** (2013) 37–43.
3. K. Sanjay, M. Miclau, C. Martin, "Hydrothermal synthesis of $AgCrO_2$ delafossite in supercritical water: A new single-step process", *Chem. Mater.*, **25** [10] (2013) 2083–2088.
4. M. Miclau, D. Grebille, C. Martin, "Crystal growth of $CaMn_{1-x}Mo_xO_3$ perovskites by the floating-zone technique ($0 \leq x \leq 0.15$)", *J. Cryst. Growth.*, **285** [4] (2005) 661–669.
5. A.E. Petrova, A.I. Pankrats, "Copper metaborate CuB_2O_4 phase diagrams based on the results of measuring the magnetic moment", *J. Exp. Theor. Phys.*, **126** [4] (2018) 506–513.
6. R. Sasaki, Y. Nii, Y. Onose, "Surface acoustic wave coupled to magnetic resonance on a multiferroic CuB_2O_4", *Phys. Rev. B*, **99** (2019) 014418.
7. J. Liu, S. Wen, X. Zou, F. Zuo, G.J.O. Beran, P. Feng, "Visible-light-responsive copper(II) borate photocatalysts with intrinsic midgap states for water splitting", *J. Mater. Chem. A*, **1** (2013) 1553–1556.
8. S. Toyod, N. Abe, T. Arima, "Gigantic directional asymmetry of luminescence in multiferroic CuB_2O_4", *Phys. Rev. B*, **93** (2016) 2011091.
9. V.V. Menshenin, "Excitons at the center of the brillouin zone in CuB_2O_4 magnetoelectric", *J. Exp. Theor. Phys.*, **124** [2] (2017) 279–285.
10. G.A. Petrakovsk, A.I. Pankrats, M.A. Popov, A.D. Balaev, D.A. Velikanov, A.M. Vorotynov, K.A. Sablina, "Magnetic properties of copper metaborate CuB_2O_4", *Low Temp. Phys.*, **28** (2002) 606–612.
11. T. Kawamata, N. Sugawara, S.M. Haidar, T. Adachi, T. Noji, K. Kudo, N. Kobayashi, Y. Fujii, H. Kikuchi, M. Chiba, G.A. Petrakovskii, M.A. Popov, L.N. Bezmaternykh, Y. Koike, "Thermal conductivity and magnetic phase diagram of CuB_2O_4", *J. Phys. Soc. Jpn.*, **88** (2019) 114708.
12. K. Imasaka, R.V. Pisarev, L.N. Bezmaternykh, T. Shimura, A.M. Kalashnikova, T. Satoh, "Excitation of multiple phonon modes in copper metaborate CuB_2O_4 via nonresonant impulsive stimulated Raman scattering", *Phys. Rev. B*, **98** (2018) 054303.
13. Y. Zheng, Z. Wang, Y. Tian, Y. Qu, S. Li, D. An, X. Chen, S. Guan, "Synthesis and performance of 1D and 2D copper borate nano/microstructures with different morphologies", *Colloid. Surface A*, **349** (2009) 156–161.
14. A.S. Kipcak, F.T. Senberber, S.A. Yuksel, E.M. Derun, S.

Piskin, "Synthesis, characterisation, electrical and optical properties of copper borate compounds", *Mater. Res. Bull.*, **70** (2015) 442–448.
15. J.D. Cuppett, S.E. Duncan, A.M. Dietrich, "Evaluation of copper speciation and water quality factors that affect aqueous copper tasting response", *Chem. Senses*, **31** (2006) 689–697.
16. N. Takeno, *Atlas of Eh-pH Diagrams. Geological Survey of Japan*, Open File Report, 2005.
17. L.N. Bezmaternykh, A.M. Potseluiko, E.A. Erlykova, I.S. Édel'man, "Optical absorption of copper metaborate CuB_2O_4", *Phys. Solid State*, **43** (2001) 309–310.
18. M.A. Butler, "Photoelectrolysis and physical properties of the semiconducting electrode WO_2", *J. Appl. Phys.*, **48** (1977) 1914–1920.
19. J. Tauc, R. Grigorovic, A. Vancu, "Optical properties and electronic structure of amorphous germanium", *Phys. Status Solidi*, **15** (1966) 627–637.
20. S.C. Neumai, R. Kaindl, R.D. Hoffmann, H. Huppertz, "The new high-pressure borate hydrate $Cu_3B_6O_{12} \cdot H_2O$", *Solid State Sci.*, **14** (2012) 229–235.
21. K. Gelderman, L. Lee, S.W. Donne, "Flat-band potential of a semiconductor: Using the Mott-Schottky equation", *J. Chem. Educ.*, **84** [4] (2007) 685–688.
22. C. Ribeiro, E.J.H. Lee, T.R. Giraldi, E. Longo, J.A. Varela, E.R. Leite, "Study of synthesis variables in the nanocrystal growth behavior of tin oxide processed by controlled hydrolysis", *J. Phys. Chem. B*, **108** (2004) 15612–15617.